

Spatial-Spectral Clustering with Anchor Graph for Hyperspectral Image

Qi Wang, *Senior Member, IEEE*, Yanling Miao, Mulin Chen, and Xuelong Li, *Fellow, IEEE*

Abstract—Hyperspectral image (HSI) clustering, which aims at dividing hyperspectral pixels into clusters, has drawn significant attention in practical applications. Recently, many graph-based clustering methods, which construct an adjacent graph to model the data relationship, have shown dominant performance. However, the high dimensionality of HSI data makes it hard to construct the pairwise adjacent graph. Besides, abundant spatial structures are often overlooked during the clustering procedure. In order to better handle the high dimensionality problem and preserve the spatial structures, this paper proposes a novel unsupervised approach called spatial-spectral clustering with anchor graph (SSCAG) for HSI data clustering. The SSCAG has the following contributions: 1) the anchor graph-based strategy is used to construct a tractable large graph for HSI data, which effectively exploits all data points and reduces the computational complexity; 2) a new similarity metric is presented to embed the spatial-spectral information into the combined adjacent graph, which can mine the intrinsic property structure of HSI data; 3) an effective neighbors assignment strategy is adopted in the optimization, which performs the singular value decomposition (SVD) on the adjacent graph to get solutions efficiently. Extensive experiments on three public HSI datasets show that the proposed SSCAG is competitive against the state-of-the-art approaches.

Index Terms—Hyperspectral image, graph-based clustering, anchor graph, spatial-spectral information.

I. INTRODUCTION

HYPERSPECTRAL image (HSI) data obtained by hyperspectral imaging spectrometer provides abundant spatial structure and spectral information of the observed objects [1], [2]. With very narrow diagnostic spectral bands (wavelength interval is generally 10 nm), HSI usually has high spectral resolution [3], and can effectively distinguish subtle objects and materials between land cover classes [4], [5]. Therefore, HSI has been applied in the real-world applications like e.g. vegetation investigation [6], resource exploration [7], environmental monitoring [8] and target identification [9]. Among current tasks, the clustering is a commonly used method for processing hyperspectral image. The purpose of HSI clustering is to partition all pixels into several groups according to their intrinsic properties. By assigning groups, the points in one group have high similarity, while those in different groups show great differences.

Though numerous techniques have been developed, HSI clustering remains to be a challenging issue. Traditional approaches include the spectral clustering [10], spectral curvature

clustering [11], the multiview clustering [12], the subspace learning [13]–[15] etc. These methods usually have high time complexity which comes from two major parts: (1) the construction of $n \times n$ adjacent graph takes $\mathcal{O}(n^2d)$, where n and d are the number of pixels and spectral bands respectively; (2) the eigenvalue decomposition on the graph Laplacian matrix costs $\mathcal{O}(n^2c)$ or $\mathcal{O}(n^3)$, where c is the number of land cover types. To address the above problems, some anchor graph-based approaches have been proposed. The Anchor Graph (AG) algorithm [16] utilizes a small number of anchors enough to cover the whole points to construct the large-scale adjacent graph. It reduces the computational complexity to $\mathcal{O}(ndm)$, where m is the number of anchors. Motivated by this, various AG-based variants have been developed over the past years [17], [18].

However, the AG-based methods ignore the spatial information within pixels, which limits their discriminant capability for real-world applications [19]. Therefore, many attempts have been made in spatial-spectral combined approaches through spatial correlations and spectral information. This category of methods mainly utilize the spatial correlations in the filtering preprocessing, which filter local homogeneous regions with single scale [20], [21]. Nevertheless, they cannot fully capture the spatial structures for two reasons: (1) the HSI data may include small and large homogeneous regions simultaneously, but the local homogeneous regions can not be covered accurately with the single-scale filter. This phenomenon makes AG-based clustering algorithms fail to describe different spatial structures of HSI; (2) most of them just consider the spatial structures in the HSI data preprocessing process, and fail to incorporate these inherent structures into the clustering process.

To overcome the aforesaid shortcomings, this paper proposes a new spatial-spectral clustering with anchor graph (SSCAG) for HSI data. The main contributions can be summarized as follows.

- We adopt the anchor graph-based strategy to construct the adjacent graph, which encodes the similarity between the data points and the anchors. Benefited from the anchor graph, the data structure is exploited effectively and the computational complexity is reduced.
- We introduce a new distance metric that skillfully combines spatial structure and spectral features, which is able to select representative neighbors. In this way, the spatial-spectral collaboration information are integrated into the proposed model.
- We design an effective neighbors assignment strategy with spatial structures to learn the adjacent graph. Different

The authors are with the School of Computer Science and the Center for OPTical IMagery Analysis and Learning (OPTIMAL), Northwestern Polytechnical University, Xi'an 710072, China (e-mail: crabwq@gmail.com, skilamiaomy1@gmail.com, chenmulin001@gmail.com, xuelong_li@nwpu.edu.cn) (*Corresponding author: Xuelong Li.*)

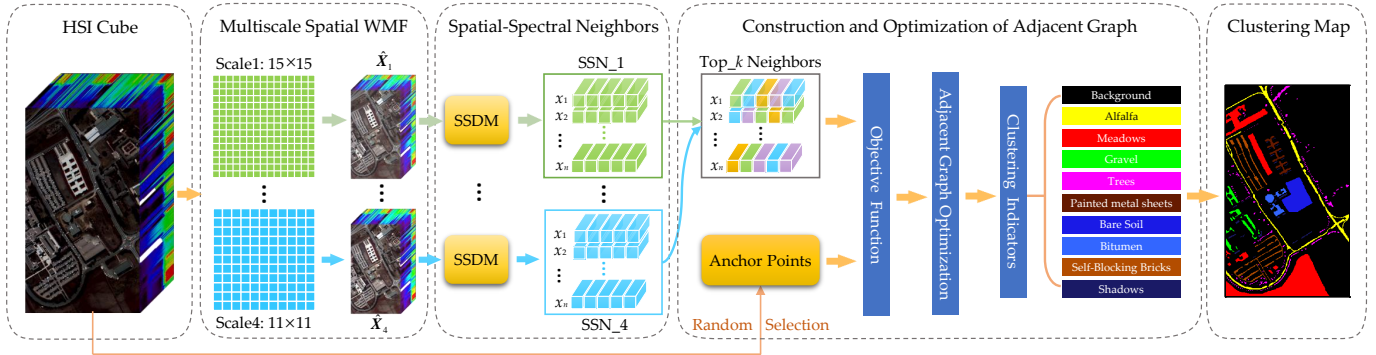


Fig. 1. Overview architecture of the proposed SSCAG. The multiscale spatial WMF first is used to process HSI data. Then the spatial-spectral neighbors of each pixel are acquired by SSDM. Next we utilize anchor points and k nearest spatial-spectral neighbors to construct objective function. By adopting an effective neighbors assignment strategy with spatial information, the final clustering is obtained. **SSDM**: spatial-spectral distance metric. **SSN_a**: spatial-spectral neighbors set.

from previous works, the proposed model employs SVD to get the final results, which is more efficient than eigenvalue decomposition.

The remainder of this paper is organized as follows. Section II introduces an overview of traditional and AG-based HSI clustering methods. Section III describes the proposed SSCAG in detail. Section IV presents the extensive experimental results and corresponding analysis. Finally, the conclusion is summarized in Section V.

II. RELATED WORK

In this section, we first briefly review the related works on traditional clustering methods, and then some existing AG-based clustering methods are introduced.

A. Traditional Clustering Methods

Many fundamental researches on HSI data clustering have been proposed. The traditional methods contains centroid-based approaches [22]–[24], density-based approaches [25], [26] and graph-based approaches [27], [28].

The centroid-based approaches usually cluster HSI data based on the similarity measure. Ren *et al.* [29] proposed an improved k -means clustering to identify the mineral types from HSI of mining area, which uses dimensionless similarity measurement methods to obtain the mapping results, enhancing spectral absorption features. Chen *et al.* [24] proposed a fuzzy c -means (FCM) clustering with spatial constraints, which contributes to the introduction of fuzziness for belongingness of each pixel and exploits the spatial contextual information. Salem *et al.* [30] developed hyperspectral feature selection for HSI clustering, which utilizes revisited FCM with spatial and spectral features to enhance the clustering. The density-based approaches form clusters by dense regions in the feature space. Tu *et al.* [31] applied density peak clustering for noisy label detection of HSI, which considers the spatial correlations of adjacent pixels to define the local densities of the training set, improving the performance of classifiers. The graph-based methods find clusters by learning the adjacent graph of data. Zhang *et al.* [27] took the spectral correlations and spatial information into sparse subspace clustering (SSC),

which obtains a more accurate coefficient matrix for building the adjacent graph and promotes the clustering performance. To overcome the single sparse representation in SSC model, Yan *et al.* [28] proposed two adjacent graph based on overall sparse representation vector and dynamic weights selection method, which better uses the spectral relationship and spatial structure during adjacent graph construction.

As mentioned above, there are some drawbacks about them. The centroid-based approaches are sensitive to initialization and noise. The density-based approaches are not suitable for HSI data, because it is hard to find density peaks in high-dimensional sparse feature space. The traditional graph-based is inefficient in large scale data, which has high computational complexity.

B. AG-based Clustering Methods

AG-based methods can address the scalability issue via a small number of anchors which adequately cover the entire points. Motivated by recent development in the AG construction, He *et al.* [17] proposed fast semi-supervised learning with AG for HSI data, which constructs a naturally sparse and scale invariant AG, alleviating the computation burden. Wang *et al.* [18] developed a scalable AG-based clustering method, which adds the non-negative relaxation to AG model. With this, the clustering results are directly obtained without adopting k -means. To handle the defect that AG-based methods usually ignore the spatial information, Wang *et al.* [32] presented fast spectral clustering with AG for HSI data, which fuses the spatial information by using the mean of neighboring pixels to reconstruct center pixel. Wei *et al.* [33] utilized the spatial correlation by adopting weighted mean filtering (WMF) to filter hyperspectral pixels, which considers the local neighborhood relationship within a window. Zhou *et al.* [20] proposed a regularized local discriminant embedding model with spatial-spectral information, which incorporates spatial feature into the dimensionality reduction procedure, to achieve optimal discriminative matrix by the minimization of local spatial-spectral scatter. Feng *et al.* [21] designed the discriminate margins with spatial-spectral neighborhood pixels, which effectively captures the discriminative features

and learns the structures of HSI data. Luo *et al.* [34] constructed the intra-class spatial-spectral hypergraph by considering the coordinate relationship and similarity between adjacent samples, which can better make the high-dimensional spatial features embedded in low-dimensional space.

III. SPATIAL-SPECTRAL CLUSTERING WITH ANCHOR GRAPH

In this section, we detail the proposed SSCAG algorithm from four aspects: weighted mean filtering (WMF), spatial-spectral neighbors, anchor-based adjacent graph construction and anchor graph-based spectral analysis. The overview architecture of SSCAG is shown in Fig. 1.

A. WMF

To smooth the homogeneous regions and reduce the interference of noisy points in the HSI, the WMF is employed to preprocess the pixels by utilizing spatial information. Suppose that each pixel of HSI can be denoted as a vector $x_i \in \mathbb{R}^d$ ($i = 1, 2, \dots, n$), where d is the number of spectral bands and n refers to the number of HSI pixels. The HSI data is denoted as $\mathbf{X} = [x_1, x_2, \dots, x_n]^T \in \mathbb{R}^{n \times d}$, and s_{ij} represents the similarity between x_i and x_j , $\mathbf{S} \in \mathbb{R}^{n \times n}$. Let $\ell(x_i) \in \{1, 2, \dots, c\}$ be the class label of the pixels $\{x_1, x_2, \dots, x_n\}$ respectively, where c is the number of classes. Assuming that the coordinate of pixel x_i is denoted as (p_i, q_i) , the adjacent pixels centered at x_i can be defined as

$$\Omega(x_i) = \left\{ x_i(p, q) \mid \begin{array}{l} p \in [p_i - t, p_i + t] \\ q \in [q_i - t, q_i + t] \end{array} \right\}, \quad (1)$$

where $t = (w - 1)/2$, w indicates the size of neighborhood window and is a positive odd number. The pixels in the neighborhood space $\Omega(x_i)$ are also represented as $\{x_{i1}, x_{i2}, \dots, x_{i(w^2-1)}\}$, where $w^2 - 1$ is the number of neighbors of x_i .

The reconstructed pixel \hat{x}_i by WMF is defined with a weighted summation, i.e.,

$$\hat{x}_i = \frac{x_i + \sum_{k=1}^{w^2-1} v_k x_{ik}}{1 + \sum_{k=1}^{w^2-1} v_k}, \quad x_{ik} \in \Omega(x_i), \quad (2)$$

where $v_k = \exp\{-\gamma_0 \|x_i - x_{ik}\|_2^2\}$ is the weight that represents the spectral similarity between x_{ik} and x_i . The parameter γ_0 is empirically set to be 0.2 in the experiments, which reflects the degree of filtering. After filtering, the consistency of pixels in the same homogeneous regions is guaranteed. Since HSI may include homogeneous regions of different sizes simultaneously, we use multiscale WMF to obtain potential spatial structures of HSI. The abundant information with multiscale complementarity is beneficial to enhance the description for local homogeneous regions, thereby improving the performance of clustering.

B. Spatial-Spectral Neighbors

To better explore the comprehensive characteristics of HSI data, we introduce a new distance metric to seek effective

neighbors by incorporating the spatial structures and spectral features.

The pixels in the HSI are spatially related [35]. Especially, the adjacent pixels in a local homogeneous area have the spatial distribution consistency of land objects, which consist of the same materials and belong to the same category [36]. Therefore, neighboring pixels are used to measure the spatial and spectral similarity. Suppose that a pixel x_i and its neighbors in $\Omega(x_i)$ form a local pixel patch $P(x_i) = \{x_{i1}, x_{i2}, \dots, x_{iw^2}\}$. Let the spatial feature matrix be $\hat{\mathbf{L}} = [l_1, l_2, \dots, l_n] \in \mathbb{R}^{2 \times n}$, where l_i denotes the coordinate of x_i . The distance d_{ss} of x_i and x_j can be defined as

$$d_{ss}(x_i, x_j) = \frac{\sum_{h=1}^{w^2} v_{ih} \|x_{ih} - \hat{x}_j\|_2}{\sum_{h=1}^{w^2} v_{ih}}, \quad x_{ih} \in P(x_i), \quad (3)$$

where v_{ih} is the weight that indicates the spatial similarity between pixel x_{ih} and \hat{x}_j . The weight can be obtained by a kernel function, which is denoted as

$$v_{ih} = \exp\left\{-\|l_{ih} - l_j\|_2^2 / \sigma_j^2\right\}, \quad (4)$$

where l_{ih} and l_j are the coordinates of x_{ih} and x_j , respectively. The spatial distance $\|l_{ih} - l_j\|_2$ is defined by the Euclidean distance between their coordinates, and σ_j is set as the average of $\sum_{h=1}^{w^2} \|l_{ih} - l_j\|_2$, i.e.,

$$\sigma_j = \frac{1}{w^2} \sum_{h=1}^{w^2} \|l_{ih} - l_j\|_2. \quad (5)$$

Note that the values of \mathbf{X} and $\hat{\mathbf{L}}$ are normalized within $[0, 1]$. Eq. (4) and Eq. (5) enforce the pixels with larger spatial distances to have a smaller similarity.

For HSI data, the spectral neighbors may contain the pixels with similar spectrum, but they are in different classes. The spatial neighbors only consider the coordinate distance of pixels, which may include pixels placed in different classes, especially at the boundary. According to Eq. (3), the proposed $d_{ss}(x_i, x_j)$ combines the spatial and spectral features simultaneously, where $\|x_{ih} - \hat{x}_j\|_2$ denotes the spectral similarity of two pixels, and v_{ih} is the corresponding spatial similarity. Furthermore, it not only considers the neighboring pixels in the patch $P(x_i)$, but also employs the adjacent pixels in the $\Omega(x_j)$. Hence, d_{ss} chooses the effective neighbors by collaborating spatial and spectral distance. After obtaining the spatial-spectral neighbors set of each pixel with different scales of WMF, we choose k nearest neighbors for constructing the objective function in the next part.

C. Anchor-based Adjacent Graph Construction

To reduce the computational complexity of constructing adjacent graph, we exploit an anchor-based strategy to learn the adjacent graph, and design an efficient strategy to accelerate the optimization. Similar to the previous works [37]–[42], the anchor-based strategy mainly consists of two steps: 1) anchors generation; 2) adjacent graph construction.

Anchors Generation: in large-scale clustering, the anchors are usually generated by k -means method or random sampling.

We employ the random selection method to generate m anchors ($m \ll n$), since its computational complexity is $\mathcal{O}(1)$. Let $\mathbf{U} = [u_1, u_2, \dots, u_m]^T \in \mathbb{R}^{m \times d}$ denotes the anchor set, and u_{ϕ_i} represents the set of k -nearest anchors for x_i .

Adjacent Graph Learning: let $\mathbf{Z} \in \mathbb{R}^{n \times m}$ be the adjacent graph, where z_{ij} denotes the similarity between x_i and u_j . \mathbf{Z} is constructed by k -nearest neighbors method. Traditional approaches usually adopt kernel-based strategy to assign neighbors [43], which always bring extra hyperparameters. Inspired by [24] and [44], we design an effective neighbor assignment strategy. The nearest anchors assignment of x_i can be seen as solving the objective function:

$$\min_{z_i^T \mathbf{1} = 1, z_{ij} \geq 0} \sum_{j=1}^m \underbrace{\|x_i - u_j\|_2^2 z_{ij}}_{\mathcal{J}_1} + \alpha \underbrace{\|\tilde{x}_i - u_j\|_2^2 z_{ij}}_{\mathcal{J}_2} + \underbrace{\gamma z_{ij}^2}_{\mathcal{J}_3}, \quad (6)$$

where z_i^T is the i -th row of \mathbf{Z} , and $\|x_i - u_j\|_2^2$ is the square of Euclidean distance between pixel x_i and anchor u_j . \tilde{x}_i denotes the average of k spatial-spectral neighbors about x_i , which can be calculated in section III-B. Similarly, $\|\tilde{x}_i - u_j\|_2^2$ is the distance between \tilde{x}_i and u_j . It can be seen that the objective function (6) contains three terms: \mathcal{J}_1 , \mathcal{J}_2 and \mathcal{J}_3 . \mathcal{J}_1 utilizes the spectral features to learn \mathbf{Z} ; \mathcal{J}_2 incorporates the local spatial-spectral feature to learn \mathbf{Z} , where α controls the tradeoff between \mathcal{J}_1 and \mathcal{J}_2 ; \mathcal{J}_3 is the regularization term, which is to prevent the trivial solution of Eq. (6), where γ is the regularization parameter.

Let us define

$$e_{ij} = \|x_i - u_j\|_2^2, \quad (7)$$

$$\tilde{e}_{ij} = \|\tilde{x}_i - u_j\|_2^2, \quad (8)$$

where $e_i \in \mathbb{R}^{m \times 1}$ denotes a vector with the j -th element as e_{ij} . Similarly, $\tilde{e}_i \in \mathbb{R}^{m \times 1}$ is a vector with the j -th element as \tilde{e}_{ij} . Combining Eq. (7) and Eq. (8), we obtain

$$E_{ij} = e_{ij} + \alpha \tilde{e}_{ij}, \quad (9)$$

and denote $E_i \in \mathbb{R}^{m \times 1}$ as a vector with the j -th element as E_{ij} , then the objective function (6) can be expressed as

$$\min_{z_i^T \mathbf{1} = 1, z_{ij} \geq 0} \frac{1}{2} \left\| z_i + \frac{1}{2\gamma} E_i \right\|_2^2. \quad (10)$$

The Lagrangian function of Eq. (10) is

$$\mathcal{L}(z_i, \eta, \beta_i) = \frac{1}{2} \left\| z_i + \frac{E_i}{2\gamma} \right\|_2^2 - \eta (z_i^T \mathbf{1} - 1) - \beta_i^T z_i, \quad (11)$$

where η and $\beta_i^T \geq 0$ are the Lagrangian multipliers. To achieve the optimal z_i^* , it should satisfy that the derivative of Eq. (11) with respect to z_i^* is equal to zero, i.e.,

$$z_i^* + \frac{E_i}{2\gamma} - \eta \mathbf{1} - \beta_i = \mathbf{0}. \quad (12)$$

Then the j -th element of z_i^* is

$$z_{ij}^* + \frac{E_{ij}}{2\gamma} - \eta \mathbf{1} - \beta_{ij} = 0. \quad (13)$$

By the KKT condition and constraints, to achieve the optimal solution z_i^* to the function (6) that has exactly k nonzero values, the η and γ are

$$\eta = \frac{1}{k} + \frac{1}{2k\gamma} \sum_{j=1}^k E_{ij}, \quad (14)$$

$$\gamma = \frac{k}{2} E_{i,k+1} - \frac{1}{2} \sum_{j=1}^k E_{ij}. \quad (15)$$

Therefore, the optimal solution z_{ij}^* is as follows:

$$z_{ij}^* = \frac{E_{i,k+1} - E_{ij}}{k E_{i,k+1} - \sum_{j'=1}^k E_{ij'}}. \quad (16)$$

For detail deviation, please refer to [44]. The calculation of z_{ij}^* only involves the basic operations: addition, subtraction, multiplication and division, which ensures the efficiency of the proposed method. In addition, there are no hyperparameters which may affect the stability of model in Eq. (16). Then, we propose to normalize \mathbf{Z} to be a doubly stochastic matrix.

Doubly Stochastic Graph Construction: after getting the adjacent graph \mathbf{Z} , the normalized adjacent graph \mathbf{S} can be computed as:

$$\mathbf{S} = \mathbf{Z} \mathbf{\Lambda}^{-1} \mathbf{Z}^T, \quad (17)$$

where $\mathbf{\Lambda}$ is a diagonal matrix whose j -th element is represented as $\Lambda_{jj} = \sum_{i=1}^n z_{ij}$, and $\mathbf{\Lambda} \in \mathbb{R}^{m \times m}$. Intuitively, the element s_{ij} of matrix \mathbf{S} is expressed as $s_{ij} = z_i^T \mathbf{\Lambda}^{-1} z_j$ that satisfies $s_{ij} = s_{ji}$. Moreover, with $z_{ij} \geq 0$ and $z_i^T \mathbf{1} = 1$, it can be proved that matrix \mathbf{S} is positive semidefinite and doubly stochastic [16]. The above property of \mathbf{S} is crucial for reducing the computation cost of optimization, and the details will be given later.

D. Anchor Graph-based Spectral Analysis

The objective function of spectral clustering is

$$\min_{\mathbf{F}^T \mathbf{F} = \mathbf{I}} \text{Tr}(\mathbf{F}^T \mathbf{L} \mathbf{F}), \quad (18)$$

where $\mathbf{F} \in \mathbb{R}^{n \times c}$ denotes clustering indicators matrix. The Laplacian matrix is $\mathbf{L} = \mathbf{D} - \mathbf{S}$, where the i -th element of the degree matrix \mathbf{D} is denoted as $d_{ii} = \sum_{j=1}^n s_{ij}$. The optimal solution of \mathbf{L} is obtained by enforcing eigenvalues decomposition on \mathbf{L} , which is comprised of eigenvectors corresponding to the smallest c eigenvalues of \mathbf{L} . However, this solution process requires $\mathcal{O}(n^2 c)$, which is not conducive to HSI clustering. According to the natural characteristics of \mathbf{S} , we have

$$d_{ii} = \sum_{j=1}^n s_{ij} = \sum_{j=1}^n z_i^T \mathbf{\Lambda}^{-1} z_j = z_i^T \sum_{j=1}^n \mathbf{\Lambda}^{-1} z_j = z_i^T \mathbf{1} = 1. \quad (19)$$

Therefore, the degree matrix \mathbf{D} equals to the identity matrix \mathbf{I} exactly. Moreover, it can be seen that the matrix \mathbf{S} is automatically normalized. Considering that $\mathbf{L} = \mathbf{D} - \mathbf{S} = \mathbf{I} - \mathbf{S}$, Eq. (18) is equivalent to solving this problem:

$$\max_{\mathbf{F}^T \mathbf{F} = \mathbf{I}} \text{Tr}(\mathbf{F}^T \mathbf{S} \mathbf{F}). \quad (20)$$

Note that \mathbf{S} can also be denoted as

$$\mathbf{S} = \mathbf{A}\mathbf{A}^T, \quad (21)$$

where $\mathbf{A} = \mathbf{Z}\mathbf{\Lambda}^{-1/2}$, then we apply SVD on \mathbf{A} as follows:

$$\mathbf{A} = \mathbf{U}\mathbf{\Sigma}\mathbf{V}^T, \quad (22)$$

where $\mathbf{U} \in \mathbb{R}^{n \times n}$, $\mathbf{\Sigma} \in \mathbb{R}^{n \times m}$ and $\mathbf{V} \in \mathbb{R}^{m \times m}$. With respect to the property of SVD, there are $\mathbf{U}^T\mathbf{U} = \mathbf{I}$ and $\mathbf{V}^T\mathbf{V} = \mathbf{I}$. So $\mathbf{S} = \mathbf{A}\mathbf{A}^T = \mathbf{U}\mathbf{\Sigma}\mathbf{V}^T\mathbf{V}\mathbf{\Sigma}^T\mathbf{U}^T = \mathbf{U}\mathbf{\Sigma}\mathbf{\Sigma}^T\mathbf{U}^T = \mathbf{U}\mathbf{\Sigma}^2\mathbf{U}^T$. It indicates that the column vectors of \mathbf{U} are the eigenvectors of \mathbf{S} . Instead of using eigenvalue decomposition on \mathbf{S} , we adopt SVD on \mathbf{A} to get the relaxed continuous solution of \mathbf{F} , which only costs $\mathcal{O}(nmc + m^2c)$. Then, we perform k -means method on \mathbf{F} to get the discrete solution.

Algorithm 1 SSCAG

Input: HSI data $\mathbf{X} \in \mathbb{R}^{n \times d}$, class number c , window size w , anchor number m , neighbor number k , the balance parameter α and $\gamma_0 = 0.2$.

- 1: **for** $i = 1$ **to** n **do**
 - 2: seek the neighbors of x_i according to Eq. (1);
 - 3: **for** $k = 1$ **to** $w^2 - 1$ **do**
 - 4: calculate the weights: $v_k = \exp\{-\gamma_0\|x_i - x_{ik}\|^2\}$;
 - 5: **end for**
 - 6: receive the filtered point \hat{x}_i by Eq. (2);
 - 7: **end for**
 - 8: Obtain $\hat{\mathbf{X}} = [\hat{x}_1, \hat{x}_2, \dots, \hat{x}_i, \dots, \hat{x}_n]$;
 - 9: **for** $i = 1$ **to** n **do**
 - 10: calculate the spatial-spectral distance d_{ss} by Eq. (3);
 - 11: find k spatial-spectral nearest neighbors for x_i , computing the average of neighbors and saving as \tilde{x}_i ;
 - 12: **end for**
 - 13: Generate m anchors by random sampling, obtaining anchor matrix $\mathbf{U} \in \mathbb{R}^{d \times m}$;
 - 14: Find k nearest neighbors of x_i in \mathbf{U} , saving the index set ϕ_i ;
 - 15: Define function $\mathcal{L}(z_i) = \|x_i - u_{\phi_i}\|_2^2 z_i + \alpha \|x_i - u_{\phi_i}\|_2^2 z_i + \gamma \|z_i\|_2^2$;
 - 16: Obtain γ and the adjacent graph \mathbf{Z} by Eq. (16) and Eq. (17);
 - 17: Design the normalized adjacent graph $\mathbf{S} = \mathbf{Z}\mathbf{\Lambda}^{-1}\mathbf{Z}^T$, $\Lambda_{jj} = \sum_{i=1}^n z_{ij}$;
 - 18: Obtain \mathbf{F} by applying SVD on matrix \mathbf{A} , and $\mathbf{A} = \mathbf{Z}\mathbf{\Lambda}^{-1/2}$;
 - 19: Utilizing k -means on \mathbf{F} for final clustering results;
- Output:** Label matrix about c classes
-

The detail steps of SSCAG are described in **Algorithm 1**. The computational complexity of **Algorithm 1** mainly comes from four parts: 1) the WMF-based spatial preprocessing takes $\mathcal{O}(ndw^2)$; 2) obtaining m anchors by random selection costs $\mathcal{O}(1)$, and the spatial-spectral combined distance d_{ss} is calculated with $\mathcal{O}(n^2w^2)$; 3) the cost of constructing \mathbf{Z} is $\mathcal{O}(ndm)$, and achieving the relaxed continuous eigenvalue of \mathbf{F} needs $\mathcal{O}(nmc + m^2c)$; 4) the k -means which is used to get the final clustering results takes $\mathcal{O}(nmc\tau)$, where τ is the number of iterations. Note that $m \ll n$, $c \ll d$, w and τ are small. Therefore, the final computational complexity of SSCAG is $\mathcal{O}(n^2w^2 + ndm)$.

IV. EXPERIMENTS

In this section, to demonstrate the effectiveness of the proposed SSCAG method, the verification experiments are conducted on public hyperspectral datasets. Some excellent algorithms are adopted as competitors. Finally, the experimental results and corresponding analysis are provided.

A. Dataset Description

The detailed information of three hyperspectral datasets are introduced as follows. Their false color images and ground truths are displayed in Fig. 2.

1) *Indian Pines*: The hyperspectral image was acquired via AVIRIS device (spatial resolution is 20 m) over the northwestern Indiana in 1992, as shown in Fig. 2 (a). The spatial size of this area is 145×145 pixels. Each pixel contains 220 spectral bands ranging from 0.4 to 2.5 μm . Due to noise and water absorption phenomena, 20 channels are removed, leaving 200 bands to be used for experiments. The dataset contains 16 land cover types, and the distribution of samples is clear in Fig. 2 (b).

2) *Pavia University*: The scene was captured by the German ROSIS sensor (spatial resolution is 1.3 m) over the Pavia in 2002, as displayed in Fig. 2 (c). The HSI data contains 610×340 pixels and 115 spectral bands, and the spectral range is 0.43 to 0.86 μm . With discarding 12 noise and water absorption bands, 103 bands are left for classification task. This dataset includes 9 ground-truth classes, and the distribution of them is shown in Fig. 2 (d).

3) *Salinas*: Like the Indian Pines image, the Salinas data was also taken by AVIRIS sensor over the Salinas Valley in 1998, as exhibited in Fig. 2 (e). Unlike Indian Pines, its spatial resolution is 3.7 m . Similarly, the 204 bands are left after excluding 20 water absorption bands. The size of Salinas image is 512×217 . All pixels in HSI data are divided into 16 categories whose distribution is illustrated in Fig. 2 (f).

B. Experimental Setup

1) *Comparison Algorithms*: To validate the superiority of the proposed SSCAG, several HSI clustering methods are considered as follows.

a) *Traditional clustering methods*: k -means [22], FCM [23] and FCM-S1 [24]. These methods are typical centroid-based clustering approaches. k -means and FCM commonly use Euclidean distance as similarity measure to achieve the clusters. k -means is a hard clustering method which assigns each sample into a certain cluster. FCM belongs to soft clustering, which uses the membership to identify the relationship between samples and each cluster. FCM-S1 has enhanced robustness of the original clustering algorithms by exploiting spatial contextual information.

b) *AG-based clustering methods*: SGCNR [18], FSCAG [32] and FSCS [33]. The first method SGCNR only adopts the spectral feature, while other methods FSCAG and FSCS consider spatial and spectral information. SGCNR builds an adjacent graph based on AG and the nonnegative relaxation conditions, which directly obtains the clustering indicators. FSCAG considers spectral correlation and spatial neighborhood properties of the HSI data to construct anchor graph. FSCS uses the spatial nearest pixels to reconstruct the center point within a window, which combines local spatial structure with spectral information.

2) *Evaluation Indices*: Three quantitative metrics are used to evaluate clustering performance, including overall accuracy (OA), average accuracy (AA) and Kappa coefficient. OA

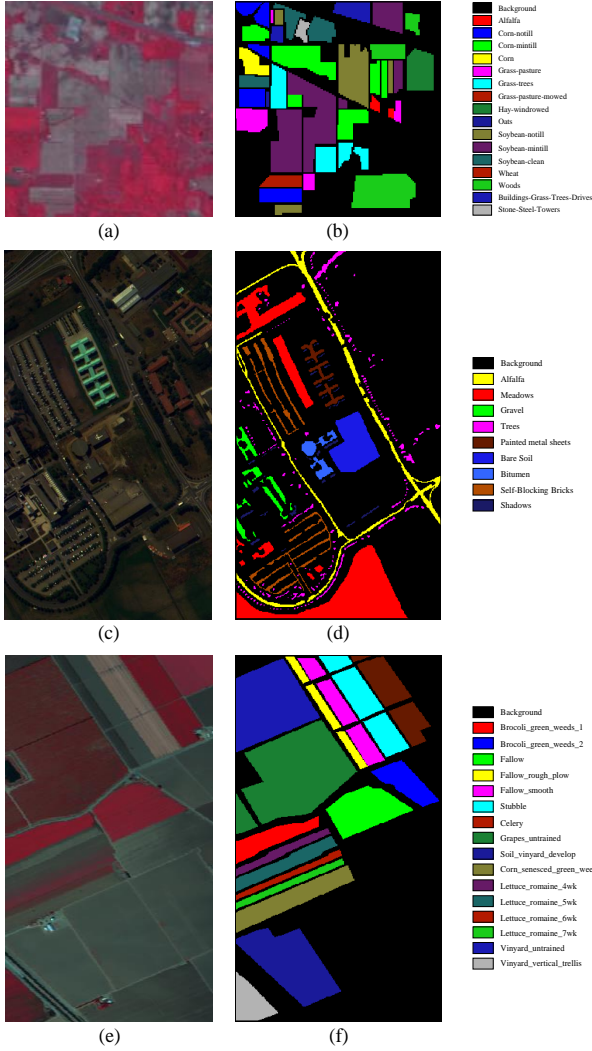


Fig. 2. The RGB false color images and ground truth maps of three HSI datasets. (a) Indian Pines image of bands 50, 27 and 17. (c) Pavia University image of bands 60, 30 and 2. (e) Salinas image of bands 70, 27 and 17. (b), (d) and (f) are corresponding ground truth maps respectively.

represents the proportion of correctly classified pixels in HSI. AA denotes the average of the classification accuracy of each category. The value of OA and AA ranges from 0 to 1. Here, the higher accuracy value, the better clustering performance. Kappa coefficient is a metric combined commission error and omission error, which can evaluate the overall consistency. Its value range is $[0,1]$. The larger Kappa values indicate better consistency.

C. Experimental Results and Analyses

1) *Parameter Settings*: The whole pixels of the Indian Pines, Pavia University and Salinas were used as testing data. Set the number of clusters equal to the number of the ground truth labels in each dataset. For centroid-based clustering methods, all the parameters are manually adjusted to the optimum. Every algorithm is repeated 20 times to avoid the bias. For AG-based methods, the optimal parameter settings of SGCNR is followed as [18]. For FSCAG, the anchors

number m , neighbors number k and balance parameter α are $\{m = 500, k = 5, \alpha = 0.6\}$ for Indian Pines, $\{m = 1000, k = 5, \alpha = 0.3\}$ for Pavia University, $\{m = 1000, k = 5, \alpha = 0.8\}$ for Salinas. For FSCS, the window size w , the anchors number m , neighbors number k and balance parameter α for three datasets are $\{w = 11, m = 500, k = 5, \alpha = 0.2\}$, $\{w = 7, m = 1000, k = 5, \alpha = 0.1\}$ and $\{w = 15, m = 1000, k = 5, \alpha = 0.2\}$. For the proposed SSCAG, we choose four different window scales, i.e., 3×3 , 7×7 , 11×11 and 15×15 , to preprocess every dataset. The corresponding parameters are set as $\{m = 500, k = 5, \alpha = 0.6\}$, $\{m = 1000, k = 5, \alpha = 0.4\}$, $\{m = 1000, k = 5, \alpha = 0.7\}$ for three HSI datasets, respectively.

2) *Clustering Performance Comparison*: In this section, experiments are conducted on three HSI datasets. The parameter analysis of the proposed approach is also discussed.

a) *Performance on Indian Pines dataset*: The quantitative results of the methods are given in Table I. It can be revealed that SSCAG obtains better results than competitors from the perspective of OA, AA and Kappa, and gains the higher accuracy in most classes. Moreover, the AG-based methods (SGCNR, FSCAG, FSCS and SSCAG) outperform the centroid-based clustering methods (k -means, FCM and FCM_S1) as shown Table I. Among these competitors, k -means and FCM are traditional clustering approaches which only focuses on the spectral information. The other algorithms (FCM_S1, FSCAG, FSCS and SSCAG) combine spectral feature and spatial structure to enforce HSI clustering. Corresponding to the Table I, the quantitative accuracy of k -means and FCM is lower (i.e., OAs reduce by at least 5%) than the accuracy of other algorithms. This reveals that incorporating spatial information is beneficial to HSI clustering. Furthermore, compared with FSCS, the proposed SSCAG improves over 10% in terms of OA. Because the WMF with multiscale windows outperforms the optimal results in single scale, which reaches higher OAs by complementary information in different scales.

To easily observe the classification of each class, we set the background of clustering maps as black color. Then the final clustering maps obtained with each algorithm are also visualized in Fig. 3. The proposed SSCAG obtains much smoother clustering maps than other methods. Especially, SSCAG has a superior performance than SGCNR and FSCAG, which indicates that WMF-based spatial preprocessing significantly provides an accurate description of HSI homogeneous areas. Moreover, the preprocessing increases OAs by enhancing the similarity and consistency of adjacent pixels. It reflects that multiscale WMF can provide more precise information for distance metric to construct an effective spatial-spectral adjacency graph in clustering procedure.

b) *Performance on Pavia University dataset*: To observe the experimental results visually and quantitatively, Fig. 4 and Table II show the visual clustering maps and the corresponding classification accuracy, respectively. As shown in Table II, the AG-based clustering methods give a superior results than the classic centroid-based methods, especially for the Bitumen class. After incorporating the spatial characteristics into the anchor graph model, FSCAG, FSCS and SSCAG yield better

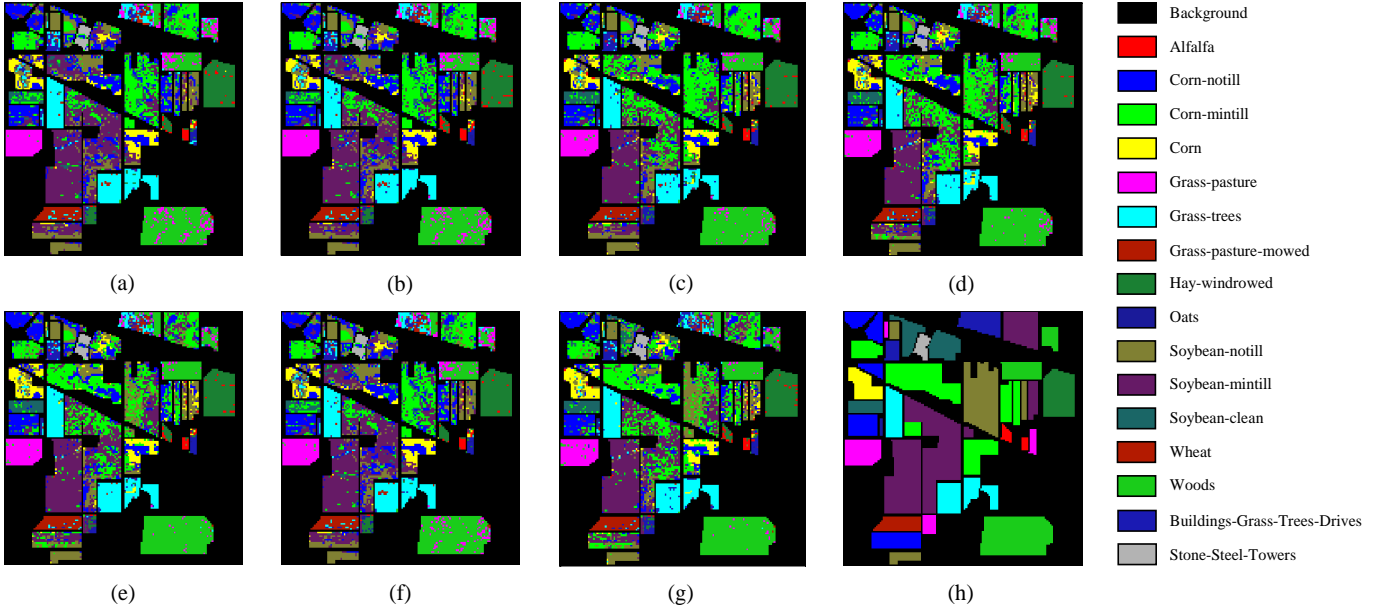


Fig. 3. Clustering maps and ground truth of Indian Pines. (a) k -means. (b) FCM. (c) FCM_S1. (d) SGCNR. (e) FSCAG. (f) FSCS. (g) SSCAG. (h) Ground truth.

TABLE I
QUANTITATIVE METRICS OF DIFFERENT COMPARISON METHODS AND THE PROPOSED SSCAG ON INDIAN PINES DATASET. THE OPTIMAL VALUE OF EACH ROW IS HIGHLIGHTED IN BOLD.

Class	k -means	FCM	FCM_S1	SGCNR	FSCAG	FSCS	SSCAG
Alfalfa	0.0872	0.2449	0.1252	0.1547	0.1143	0.0187	0.1749
Corn-notill	0.2049	0.2701	0.2334	0.2765	0.3397	0.3245	0.4097
Corn-mintill	0.1424	0.1606	0.3404	0.4131	0.4190	0.1467	0.4431
Corn	0.1612	0.1689	0.1466	0.2079	0.3051	0.2236	0.5402
Grass-pasture	0.6067	0.6539	0.6099	0.5928	0.5373	0.5983	0.5039
Grass-trees	0.7278	0.7082	0.6988	0.7124	0.7987	0.7837	0.8395
Grass-pasture-mowed	0.8081	0.8215	0.7985	0.7548	0.7665	0.8004	0.7829
Hay-windrowed	0.8602	0.7952	0.8727	0.8825	0.8573	0.9282	0.8571
Oats	0.3501	0.4302	0.4500	0.4459	0.3535	0.4315	0.3462
Soybean-notill	0.1558	0.1798	0.292	0.2735	0.3501	0.2925	0.4543
Soybean-mintill	0.6307	0.5381	0.4792	0.3934	0.4038	0.5605	0.5033
Soybean-clean	0.0598	0.1083	0.2124	0.2753	0.2590	0.1192	0.3531
Wheat	0.8086	0.8107	0.8244	0.8261	0.8438	0.8356	0.8617
Woods	0.4012	0.4145	0.4495	0.4877	0.7863	0.4949	0.8503
Buildings-Grass-Trees-Drives	0.1288	0.1436	0.3054	0.2881	0.1716	0.0736	0.2877
Stone-Steel-Towers	0.7161	0.7017	0.7845	0.8182	0.8042	0.7957	0.8867
OA	0.3929	0.4128	0.4551	0.4531	0.4708	0.4409	0.5427
AA	0.4281	0.4469	0.4764	0.4877	0.5069	0.4642	0.5684
Kappa	0.3241	0.3512	0.3709	0.3931	0.4019	0.3816	0.4818

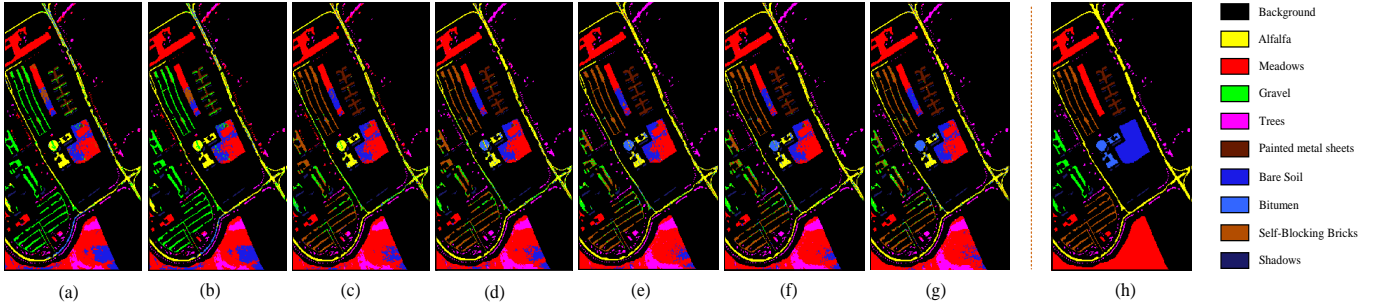


Fig. 4. Clustering maps and ground truth of Pavia University. (a) k -means. (b) FCM. (c) FCM_S1. (d) SGCNR. (e) FSCAG. (f) FSCS. (g) SSCAG. (h) Ground truth.

TABLE II
QUANTITATIVE METRICS OF DIFFERENT COMPARISON METHODS AND THE PROPOSED SSCAG ON PAVIA UNIVERSITY DATASET. THE OPTIMAL VALUE OF EACH ROW IS HIGHLIGHTED IN BOLD.

Class	k -means	FCM	FCM_S1	SGCNR	FSCAG	FSCS	SSCAG
Asphalt	0.7431	0.7525	0.6827	0.6289	0.8411	0.8598	0.8378
Meadows	0.6403	0.6395	0.6791	0.7521	0.8141	0.8090	0.8245
Gravel	0.9827	0.9877	0.4369	0.2857	0.5331	0.5089	0.5440
Trees	0.6363	0.6220	0.6152	0.7892	0.7116	0.7313	0.7908
Painted metal sheets	0.5424	0.5438	0.9865	0.9728	0.9956	0.9548	0.9738
Bare Soil	0.3019	0.2755	0.3106	0.3897	0.3570	0.4007	0.4461
Bitumen	0	0	0	0.2915	0.5708	0.5774	0.5813
Self-Blocking Bricks	0.0014	0.0039	0.6535	0.8621	0.6996	0.6648	0.7451
Shadows	0.9978	0.9975	0.9969	0.9980	1.0000	1.0000	1.0000
OA	0.5340	0.5341	0.5746	0.6275	0.7306	0.7089	0.7504
AA	0.5384	0.5358	0.5957	0.6633	0.7248	0.7230	0.7493
Kappa	0.4336	0.4334	0.4546	0.5751	0.6497	0.6324	0.6747

accuracy in almost all classes compared with SGCNR, particularly for the Shadows class. This indicates that the combination of spatial and spectral information is beneficial to improve HSI clustering performance. The proposed SSCAG obtains the best results for 5 classes, except for the Gravel class, which also achieves better accuracy for other 3 classes. The OA and kappa coefficient of SSCAG achieves to 0.7504 and 0.6747, respectively. It illustrates that SSCAG is an effective and superior algorithm for HSI clustering. As is shown in Fig. 4, SSCAG gains more smoother clustering map than other methods, which is consistent with the results in Table II.

c) Performance on Salinas dataset: To visualize the experimental results, the clustering maps are illustrated in Fig. 5. The quantitative accuracy of comparison algorithms and SSCAG are exhibited in Table III. According to the visual results, it reveals that the pixels in the Grapes_untrained class and Vinyard_untrained class regions are most wrongly assigned. That is because the Grapes_untrained and Vinyard_untrained have highly similar feature information, and their spectral curves are very close. From Fig. 5 (g), the Lettuce_roumaine_7wk class is discriminated well, and its accuracy reaches to 0.9042 in Table III, which is higher than that of other methods. As shown in Table III, the results indicate that the proposed SSCAG yields the best classification accuracies, especially the

OA and Kappa coefficient are 0.7419 and 0.6993 respectively. Furthermore, it can be observed that the Lettuce_4wk class is effectively assigned by SSCAG, in contrast, the recognition accuracy of other algorithms except SGCNR is close to 0. This phenomenon also justifies the effectiveness of SSCAG.

d) Parameter Analysis: The proposed SSCAG contains four parameters that need to be set and tuned, i.e. m , w , k and α . As mentioned in Section III, the computational complexity mainly depends on the size of parameters m and w . The parameter k mainly controls the sparsity of matrix \mathbf{Z} , which affects the computational complexity little. Concretely, we implement the sensitivity experiments of m and k on Indian Pines dataset.

According to Fig. 6 (a), the fluctuation range of OAs is small. We can see that the OAs of the proposed SSCAG are relatively stable with changing the parameters m and k . As shown in Fig. 6 (b), the running time is mainly related to m , while the influence of k is little. Hence, to speed up SSCAG algorithm and ensure good accuracy, we choose $\{m = 500, k = 5\}$ for the Indians Pines dataset. Similarly, we select $\{m = 1000, k = 5\}$ for the other large datasets.

Fig. 6 (c) illustrates the OAs of three HSI datasets with varying α . α is an important parameter in SSCAG, which is used to adjust the tradeoff between spectral feature and spatial-spectral feature during the adjacent graph learning. From Fig.

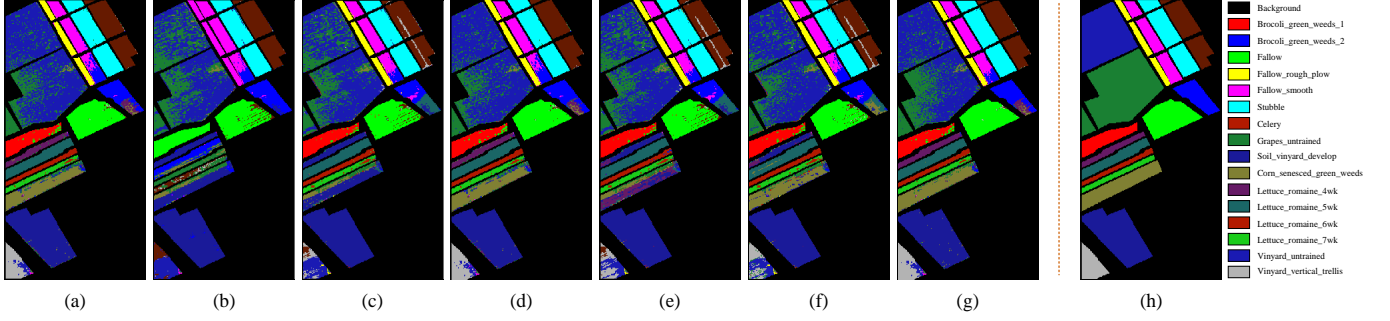


Fig. 5. Clustering maps and ground truth of Salinas. (a) k -means. (b) FCM. (c) FCM_S1. (d) SGCNR. (e) FSCAG. (f) FSCS. (g) SSCAG. (h) Ground truth.

TABLE III
QUANTITATIVE METRICS OF DIFFERENT COMPARISON METHODS AND THE PROPOSED SSCAG ON SALINAS DATASET. THE OPTIMAL VALUE OF EACH ROW IS HIGHLIGHTED IN BOLD.

Class	k -means	FCM	FCM_S1	SGCNR	FSCAG	FSCS	SSCAG
Brocoli_green_weeds_1	0.8677	0	0.9826	0.9501	0.9474	0.9300	0.9204
Brocoli_green_weeds_2	0.4556	0.9010	0.4367	0.5203	0.3695	0.4610	0.5678
Fallow	0.7586	0.7070	0.7071	0.7825	0.7125	0.7376	0.8820
Fallow_rough_plow	0.9484	0	0.9819	0.9241	0.9579	0.9507	0.9087
Fallow_smooth	0.7788	0.8545	0.8972	0.7088	0.8496	0.8578	0.8985
Stubble	0.9649	0.9465	0.9545	0.959	0.9587	0.9518	0.9790
Celery	0.9042	0.9863	0.9055	0.9388	0.8847	0.8860	0.9117
Grapes_untrained	0.1820	0.3780	0.4133	0.3415	0.4486	0.3817	0.4626
Soil_vinyard_develop	0.8001	0.9713	0.9164	0.7917	0.8710	0.8538	0.8336
Corn_senesced_green_weeds	0.5245	0.3785	0.2739	0.5023	0.3239	0.5946	0.6199
Lettuce_romaine_4wk	0.2849	0.0024	0	0.6526	0.1083	0.2314	0.8968
Lettuce_romaine_5wk	0.8789	0.2229	0.9889	0.9953	0.9805	0.8954	0.9525
Lettuce_romaine_6wk	0.9513	0.1069	0.9782	0.9536	0.7888	0.9847	0.9480
Lettuce_romaine_7wk	0.4598	0.5879	0.8457	0.8501	0.8557	0.8944	0.9042
Vinyard_untrained	0.6340	0.5065	0.6295	0.6982	0.5506	0.5631	0.6385
Vinyard_vertical_trellis	0.4186	0.0682	0.2561	0.5058	0.4161	0.4802	0.5825
OA	0.6438	0.4623	0.6754	0.7208	0.6569	0.7053	0.7419
AA	0.6758	0.4761	0.6980	0.7547	0.6890	0.7284	0.8067
Kappa	0.6214	0.4038	0.5907	0.6771	0.6216	0.6676	0.6993

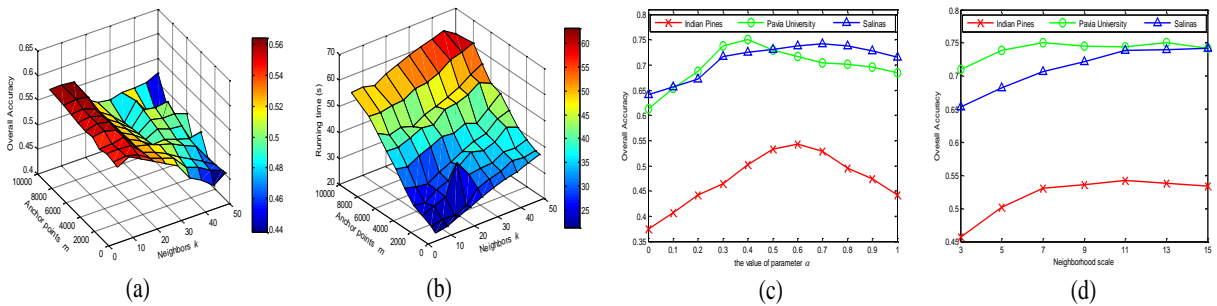


Fig. 6. Parameter analysis in different situations. (a) OAs of SSCAG on Indian Pines dataset under different m and k . (b) Running time of SSCAG on Indian Pines dataset under different m and k . (c) OAs of SSCAG on three datasets with different values of α . (d) Effects of the scale w on datasets.

TABLE IV
RUNNING TIME OF DIFFERENT METHODS ON THREE HSI DATASETS

Dataset	k -means	FCM	FCM_S1	SGCNR	FSCAG	FSCS	SSCAG
Indian Pines	5.6s	7.1s	9.6s	10.6s	10.1s	9.9s	21.3s
Pavia University	26.3s	36.7s	49.3s	121.7s	137.5s	191s	130.8s
Salinas	20.1s	27.4s	37.7s	45.8s	26s	25.7	61.1s

6 (c), the result demonstrates that the optimal value of α is 0.6, 0.4 and 0.7 for Indian Pines, Pavia University and Salinas datasets, respectively. Fig. 6 (d) exhibits the OAs of three datasets with seven different neighborhood scales. The parameter w is the window scale of WMF that affects the result of preprocessing. Here, we adopt seven different scales (i.e., 3×3 , 5×5 , ..., 15×15) to investigate its impact. As shown in Fig. 6 (d), the best OAs for Indian Pines, Pavia University and Salinas are obtained, when the window scale is 11, 7 and 15 respectively. This indicates that different HSI datasets involve different spatial structures, even the same dataset may include small and large homogeneous regions simultaneously. So it is difficult to determine a best scale in advance. Therefore, we adopt four scales (3×3 , 7×7 , 11×11 and 15×15) in the multiscale WMF framework, which not only exempts from the scale selection but also provides multiple views of a local homogeneous region. By doing this, it obtains the complementary information and improve the final clustering performance.

3) *Running Time Comparison*: We display the running time to quantitatively compare the complexity of all algorithms, as shown in Table IV. All of the experimental results are conducted in MATLAB R2014a on a PC of Intel Core i7-9700F 3.00GHz CPU with 16 GB RAM. As shown in Table IV, k -means consumes the least running time, but its accuracy is generally not high comparing with other algorithms (see Table I, II and III). From Table IV, the proposed SSCAG method is slower than the other algorithms on the HSI datasets except Pavia University dataset. However, according to Table I, II and III, SSCAG provides best results than other methods, especially for AAs, which are 6%, 2.5% and 5% higher than the second best results on Indian Pines, Pavia University and Salinas datasets respectively. Therefore, the slight increase in running time is acceptable for the improvement in clustering performance.

V. CONCLUSION

In this paper, a novel spatial-spectral clustering with anchor graph (SSCAG) is proposed to efficiently cluster HSI data. Firstly, the multiscale spatial WMF is utilized to enhance the local pixel consistency and distinguish the structures across different classes. To facilitate the graph construction, we select representative anchors and exploit their relationship with the points, which reduces the computational complexity of model. Secondly, a new spatial-spectral distance metric is proposed to combine the comprehensive features, which reveals the inherent properties of HSI data. Finally, the neighbors assignment strategy is used to learn the optimal adjacent graph adaptively,

and SVD is performed on \mathbf{S} to get the final clustering results. Extensive experiments on three public HSI datasets verify the efficiency and effectiveness of the proposed SSCAG. In the future, we mainly focus on designing a fusion strategy with multi-graph construction to better handle the tasks of HSI clustering.

REFERENCES

- [1] Linlin Xu, Alexander Wong, Fan Li, and David A Clausi, "Intrinsic representation of hyperspectral imagery for unsupervised feature extraction," *IEEE Transactions on Geoscience and Remote Sensing*, vol. 54, no. 2, pp. 1118–1130, 2015.
- [2] Q. Wang, Q. Li, and X. Li, "A fast neighborhood grouping method for hyperspectral band selection," *IEEE Transactions on Geoscience and Remote Sensing*, 2020.
- [3] Cheng Deng, Xianglong Liu, Chao Li, and Dacheng Tao, "Active multi-kernel domain adaptation for hyperspectral image classification," *Pattern Recognition*, vol. 77, pp. 306–315, 2018.
- [4] Q. Wang, Z. Meng, and X. Li, "Locality adaptive discriminant analysis for spectral-spatial classification of hyperspectral images," *IEEE Geoscience and Remote Sensing Letters*, vol. 14, no. 11, pp. 2077–2081, 2017.
- [5] Shaohui Mei, Junhui Hou, Jie Chen, Lap-Pui Chau, and Qian Du, "Simultaneous spatial and spectral low-rank representation of hyperspectral images for classification," *IEEE Transactions on Geoscience and Remote Sensing*, vol. 56, no. 5, pp. 2872–2886, 2018.
- [6] S. Susan, S. Shinde, and S. Batra, "Vegetation-specific hyperspectral band selection for binary-to-multiclass classification," in *Proceedings of IEEE 16th India Council International Conference*, 2019, pp. 1–4.
- [7] F. Gan, S. Liang, P. Du, F. Dang, K. Tan, H. Su, and Z. Xue, "Chesre: A comprehensive public hyperspectral experimental site and data set for resources exploration," in *Proceedings of the 7th Workshop on Hyperspectral Image and Signal Processing: Evolution in Remote Sensing*, 2015, pp. 1–4.
- [8] Y. Wan, X. Hu, Y. Zhong, A. Ma, L. Wei, and L. Zhang, "Tailings reservoir disaster and environmental monitoring using the uav-ground hyperspectral joint observation and processing: A case of study in xinjiang, the belt and road," in *IEEE International Geoscience and Remote Sensing Symposium*, 2019, pp. 9713–9716.
- [9] Qi Wang, Zhenghang Yuan, Qian Du, and Xuelong Li, "GETNET: A general end-to-end two-dimensional CNN framework for hyperspectral image change detection," *IEEE Transactions on Geoscience and Remote Sensing*, vol. 57, no. 1, pp. 3–13, 2019.
- [10] Andrew Y Ng, Michael I Jordan, and Yair Weiss, "On spectral clustering: Analysis and an algorithm," in *Advances in neural information processing systems*, 2002, pp. 849–856.
- [11] Guangliang Chen and Gilad Lerman, "Spectral curvature clustering (scc)," *International Journal of Computer Vision*, vol. 81, no. 3, pp. 317–330, 2009.
- [12] Xuelong Li, Mulin Chen, Feiping Nie, and Qi Wang, "A multiview-based parameter free framework for group detection," in *Proceedings of the Thirty-First AAAI Conference on Artificial Intelligence*, 2017, pp. 4147–4153.
- [13] H. Zhang, H. Zhai, L. Zhang, and P. Li, "Spectral-spatial sparse subspace clustering for hyperspectral remote sensing images," *IEEE Transactions on Geoscience and Remote Sensing*, vol. 54, no. 6, pp. 3672–3684, 2016.
- [14] Xuelong Li, Mulin Chen, Feiping Nie, and Wang Qi, "Locality adaptive discriminant analysis," in *Proceedings of the Twenty-Sixth International Joint Conference on Artificial Intelligence*, 2017, pp. 2201–2207.

- [15] Jianing Xi, Xiguo Yuan, Minghui Wang, Ao Li, Xuelong Li, and Qinghua Huang, "Inferring subgroup specific driver genes from heterogeneous cancer samples via subspace learning with subgroup indication," *Bioinformatics*, vol. 36, pp. 1855–1863, 2020.
- [16] Wei Liu, Junfeng He, and Shih-Fu Chang, "Large graph construction for scalable semi-supervised learning," in *Proceedings of the 27th International Conference on Machine Learning*, 2010, pp. 679–686.
- [17] F. He, R. Wang, and W. Jia, "Fast semi-supervised learning with anchor graph for large hyperspectral images," *Pattern Recognition Letters*, vol. 130, pp. 319–326, 2020.
- [18] Rong Wang, Feiping Nie, Zhen Wang, Fang He, and Xuelong Li, "Scalable graph-based clustering with nonnegative relaxation for large hyperspectral image," *IEEE Transactions on Geoscience and Remote Sensing*, vol. 57, no. 10, pp. 7352–7364, 2019.
- [19] Hong Huang, Guangyao Shi, Haibo He, Yule Duan, and Fulin Luo, "Dimensionality reduction of hyperspectral imagery based on spatial-spectral manifold learning," *IEEE Transactions on Cybernetics*, vol. 50, no. 6, pp. 2604–2616, 2019.
- [20] Yicong Zhou, Jiangtao Peng, and CL Philip Chen, "Dimension reduction using spatial and spectral regularized local discriminant embedding for hyperspectral image classification," *IEEE Transactions on Geoscience and Remote Sensing*, vol. 53, no. 2, pp. 1082–1095, 2014.
- [21] Zhixi Feng, Shuyuan Yang, Shigang Wang, and Licheng Jiao, "Discriminative spectral-spatial margin-based semisupervised dimensionality reduction of hyperspectral data," *IEEE Geoscience and Remote Sensing Letters*, vol. 12, no. 2, pp. 224–228, 2014.
- [22] John A Hartigan and Manchek A Wong, "Algorithm as 136: A k-means clustering algorithm," *Journal of the royal statistical society. series c (applied statistics)*, vol. 28, no. 1, pp. 100–108, 1979.
- [23] James C Bezdek, Robert Ehrlich, and William Full, "Fcm: The fuzzy c-means clustering algorithm," *Computers and Geosciences*, vol. 10, no. 2-3, pp. 191–203, 1984.
- [24] Songcan Chen and Daoqiang Zhang, "Robust image segmentation using fcm with spatial constraints based on new kernel-induced distance measure," *IEEE Transactions on Systems, Man, and Cybernetics, Part B (Cybernetics)*, vol. 34, no. 4, pp. 1907–1916, 2004.
- [25] Alex Rodriguez and Alessandro Laio, "Clustering by fast search and find of density peaks," *Science*, vol. 344, no. 6191, pp. 1492–1496, 2014.
- [26] Singh Vijendra, "Efficient clustering for high dimensional data: Subspace based clustering and density based clustering," *Information Technology Journal*, vol. 10, no. 6, 2011.
- [27] Hongyan Zhang, Han Zhai, Liangpei Zhang, and Pingxiang Li, "Spectral-spatial sparse subspace clustering for hyperspectral remote sensing images," *IEEE Transactions on Geoscience and Remote Sensing*, vol. 54, no. 6, pp. 3672–3684, 2016.
- [28] Qing Yan, Yun Ding, Jing Jing Zhang, Yi Xia, and Chun Hou Zheng, "A discriminated similarity matrix construction based on sparse subspace clustering algorithm for hyperspectral imagery," *Cognitive Systems Research*, vol. 53, pp. 98–110, 2019.
- [29] Z. Ren, L. Sun, Q. Zhai, and X. Liu, "Mineral mapping with hyperspectral image based on an improved k-means clustering algorithm," in *IEEE International Geoscience and Remote Sensing Symposium*, 2019, pp. 2989–2992.
- [30] Manel Ben Salem, Karim Ettaba, and Med Bouhleh, "Hyperspectral image feature selection for the fuzzy c-means spatial and spectral clustering," in *Image Processing, Applications and Systems*, 2016, pp. 1–5.
- [31] B. Tu, X. Zhang, X. Kang, J. Wang, and J. A. Benediktsson, "Spatial density peak clustering for hyperspectral image classification with noisy labels," *IEEE Transactions on Geoscience and Remote Sensing*, vol. 57, no. 7, pp. 5085–5097, 2019.
- [32] Rong Wang, Feiping Nie, and Weizhong Yu, "Fast spectral clustering with anchor graph for large hyperspectral images," *IEEE Geoscience and Remote Sensing Letters*, vol. 14, no. 11, pp. 2003–2007, 2017.
- [33] Yiwei Wei, Chao Niu, Yiting Wang, Hongxia Wang, and Daizhi Liu, "The fast spectral clustering based on spatial information for large scale hyperspectral image," *IEEE Access*, vol. 7, pp. 141045–141054, 2019.
- [34] Fulin Luo, Bo Du, Liangpei Zhang, Lefei Zhang, and Dacheng Tao, "Feature learning using spatial-spectral hypergraph discriminant analysis for hyperspectral image," *IEEE transactions on cybernetics*, vol. 49, no. 7, pp. 2406–2419, 2018.
- [35] Q. Wang, X. He, and X. Li, "Locality and structure regularized low rank representation for hyperspectral image classification," *IEEE Transactions on Geoscience and Remote Sensing*, vol. 57, no. 2, pp. 911–923, 2019.
- [36] Hongyan Zhang, Han Zhai, Liangpei Zhang, and Pingxiang Li, "Spectral-spatial sparse clustering for hyperspectral remote sensing images," *IEEE Transactions on Geoscience and Remote Sensing*, vol. 54, no. 6, pp. 3672–3684, 2016.
- [37] Cheng Deng, Rongrong Ji, Wei Liu, Dacheng Tao, and Xinbo Gao, "Visual reranking through weakly supervised multi-graph learning," in *Proceedings of the IEEE International Conference on Computer Vision*, 2013, pp. 2600–2607.
- [38] Cheng Deng, Rongrong Ji, Dacheng Tao, Xinbo Gao, and Xuelong Li, "Weakly supervised multi-graph learning for robust image reranking," *IEEE transactions on multimedia*, vol. 16, no. 3, pp. 785–795, 2014.
- [39] Deng Cai and Xinlei Chen, "Large scale spectral clustering via landmark-based sparse representation," *IEEE transactions on cybernetics*, vol. 45, no. 8, pp. 1669–1680, 2014.
- [40] Feiping Nie, Wei Zhu, and Xuelong Li, "Unsupervised large graph embedding," in *Proceedings of the Thirty-First AAAI Conference on Artificial Intelligence*, 2017, pp. 2422–2428.
- [41] Feiping Nie, Wei Zhu, and Xuelong Li, "Unsupervised large graph embedding based on balanced and hierarchical k-means," *IEEE Transactions on Knowledge and Data Engineering*, 2020.
- [42] Xuelong Li, Mulin Chen, and Qi Wang, "Adaptive consistency propagation method for graph clustering," *IEEE Transactions on Knowledge and Data Engineering*, vol. 32, no. 4, pp. 797–802, 2019.
- [43] Trevor Hastie, Robert Tibshirani, and Jerome Friedman, *The elements of statistical learning: data mining, inference, and prediction*, Springer Science & Business Media, 2009.
- [44] Feiping Nie, Xiaoqian Wang, Michael I Jordan, and Heng Huang, "The constrained laplacian rank algorithm for graph-based clustering," in *Proceedings of the Thirtieth AAAI Conference on Artificial Intelligence*. Citeseer, 2016, pp. 1969–1976.